An experimental investigation of jet noise from septa nozzles

K.B.M.Q. Zaman[1], J.E. Bridges[2], A. F. Fagan[3] and C. A. Brown[4]
NASA Glenn Research Center
Cleveland, OH 44135

Abstract
Results of an experimental study with a large aspect ratio rectangular nozzle, divided into multiple compartments or septa, as pertinent to distributed propulsion, are presented. Noise measurements at high-subsonic conditions show that the nozzle with the septa is quieter than the corresponding baseline nozzle without the septa. At relatively lower Mach numbers a high-frequency tone is heard. This is shown to be due to Karmann vortex shedding from the trailing edge of the partitions that separate a septum from the adjacent ones. Flowfield measurements for a six septa case show that the cellular flow structure, issuing from the nozzle, goes through a curious coalescence with increasing downstream distance (x) from the nozzle. Adjacent cells pair to yield a three-cell structure by x/D =2, where D is the equivalent diameter of the baseline nozzle. By about x/D =16, both the septa case and the baseline case evolve to yield axisymmetric flowfields.

1. Introduction

The present investigation was prompted by nozzle requirements for the concept of a distributed propulsion system [1, 2]. The concept is driven by a potential for performance (efficiency) improvement. It involves a nozzle that is of large aspect ratio rectangular shape but divided into multiple septa (compartments). In one version of the concept, each septum is driven by an electric fan. The power comes from gas turbine engines driving electric motors and integrated suitably with the airframe. System studies have shown various advantages with such hybrid propulsion. However, from the aeroacoustics point of view there are concerns. Additional noise, relative to the noise from an equivalent single nozzle, may be produced. Also, jets placed side by side sometimes go into resonance producing tones. There are many other questions and concerns regarding the optimum septa geometry from performance as well as aeroacoustics points of view. In order to address these, an investigation was initiated at NASA Glenn Research Center (GRC). Plans were under way for conducting experiments with realistic hardware in the Center's Aeroacoustic Propulsion Laboratory (AAPL). In support of this and for preliminary explorations with a basic septa nozzle (without the fans), a study was conducted with model-scale hardware in a smaller jet facility. Limited noise measurements and flowfield surveys were conducted while varying several geometric and flow parameters. The results of this model-scale experiment, together with confirmation noise data from a brief experiment in the AAPL with the same nozzle hardware, are presented in this paper.

2. Experimental Facility and Procedure

An open jet facility (referred to as, 'CW17') at NASA GRC is used for most of this experiment. Compressed air passes through a 30" diameter plenum chamber before exhausting through the nozzle into the ambient of the test chamber. Only cold (unheated) flows are considered and further description of the facility can be found in earlier publications, e.g., [3]. The compressed air supply comes from a central system and up to 70 psig pressures are permitted. The facility also has an auxiliary blower that can provide low subsonic flow up to a jet Mach number of 0.32. The latter is used for detailed flowfield surveys using hot-wire anemometry. With a suitable adapter, the same nozzles used in the AAPL can be investigated in this facility and vice versa. An 8:1 aspect ratio nozzle, referred to as 'NA8Z' [4], is used. The nozzle exit has dimensions of 5.34"x0.66" and thus an equivalent diameter, D=2.12". A picture of the jet facility is shown in Fig. 1(a). Figure 1(b)

[1] Inlets & Nozzles Branch, Propulsion Division.
[2] Acoustics Branch, Propulsion Division.
[3] Optics and Photonics Branch, Communication and Intelligent Systems Division.
[4] Acoustics Branch, Propulsion Division.

shows another view with the setup for hot-wire measurements. The coordinate origin is placed at the center of the nozzle exit with *x* denoting distance downstream; positive *y* is to the right and positive z vertically up. Thus, the nozzle major axis is aligned with the z-axis in Fig. 1(a) while it is aligned with the y-axis in Fig. 1(b).

The septa geometry is created by placing an insert inside the nozzle. The insert is designed to fit snugly into the nozzle and is held in place under flow because of the convergent geometry of the nozzle. Various designs of the septa are explored and these are fabricated by 3-D printing. A picture of a set of inserts is shown in Fig. 1(c). In this set, all inserts have 6 septa. Each septum starts with a rectangular entrance, converges to a circular passage, and ends with an almost square shape. The design is such that the flow always converges up to the exit. This internal geometry will be referred to as 'design I' (Fig. 1d). Unless stated otherwise, all data will pertain to this design. In order to explore a tone due to vortex shedding from the partitions separating the septa, another set of inserts was fabricated. For this case, the number of septa was varied and each septum had rectangular passages throughout without a transition through a circular cross-section. This internal geometry will be referred to as 'design II' (Fig. 1d). Only limited data are presented with the latter design. As will be shown with the flowfield results, this design change made a significant impact on the flowfield downstream although the trailing edge (TE) shedding tone was persistent with either design.

The walls of the insert are as thin as permitted by the 3-D printing machines (near the exit the walls are typically 0.050" thick.). The walls and partitions result in flow blockage. The equivalent diameter of the exit with an insert is about 1.90", 11% smaller than that of the baseline (no insert) case. Schematics of the exit geometries of the eight inserts of Fig. 1(c) together with that of the baseline (no-insert) case are shown in Fig. 2. The septa cases resulted in a noise reduction relative to the baseline case, as illustrated in the following. The various exit geometries were explored for maximum noise reduction. Abbreviations used to denote the various cases are listed in the caption of Fig. 2. As stated already, each septum in this set has rectangular-to-circular-to-rectangular passage. While the baseline case is denoted as 'Bsln', case #2 involves partitions ending flush with the exit and is denoted as 'Flsh'. In case #3 (Insd), each partition is recessed and ends 0.25" inside of the exit. In case #4 (OutF), the partitions with full width protrude 0.175" from the exit. Case#5 (OutT) is similar to case#4 but the ends of the partitions past the exit are trimmed and spans 75% of the width. The scalloped (Sclp) case is the same as the Flsh case but there is a semicircular cutout at the end of each partition spanning 75% of the width. Each tab in cases #7-9, has 0.25" base with 90°-apex and are inclined into the flow by roughly 15°. The 3-D printing was not precise and the dimensions quoted are approximate. Most of the data in the following will be for case#2 (Flsh) as compared to the baseline (Bsln) case.

The test cell has acoustic linings on the ceiling and upper walls that enable qualitative noise measurements. For the present study, comparative spectral levels from geometry to geometry are examined and the facility is considered adequate for that purpose. As it will be shown, the inferences drawn are confirmed by a brief experiment, with the same nozzle and inserts, in the AAPL. The latter facility is anechoic and permits detailed and accurate noise measurements over full ranges of polar and azimuthal angles. In CW17, microphones (¼", B&K 4135) held fixed on an overhead arm are used to obtain the noise data. The microphone polar location θ is referenced with respect to the jet's downstream axis. Data for two θ locations, 90° and 25°, will be shown. The distances of the microphones from the center of the nozzle exit are 49" and 85", respectively. The microphones are overhead and thus they are located on the major axis plane of the nozzle with respect to the configuration shown in Fig. 1(a) , (ϕ=90°). Data on the minor axis plane, i.e., microphones located on the broadside (ϕ=0°), were obtained by rotating the nozzle by 90°. Spectral analysis is done over 0-50kHz with a bandwidth of 62.5 Hz. Unless stated otherwise, the spectral data will pertain to microphones located on the minor axis plane (ϕ=0°). For the CW17 noise data, the relative levels are the focus and the results will be shown as measured without any correction or normalization.

A focusing schlieren system is used for flow visualization. The system is based on a lens and grid technique where a source grid is projected onto a retro-reflective screen and imaged onto a cut-off grid creating the schlieren effect; an interested reader may find details starting with ref. [5]. The light source illuminating the

flowfield has 1-microsecond pulse duration. All optical components, as well as the scientific-grade charged-coupled-device (CCD) camera are housed in a 23"x17"x10" case. The case is placed on one side of the jet while the 30" x 24" retro-reflective screen is placed on the other side. The distances of the two items dictate the size of the field of view. The chosen distances, within the constraints of the test chamber, provide a field of view that extends approximately 9" in the streamwise direction. The thickness of the focused field is estimated to be about 3".

A jet Mach number (M_j) range from 0.5 to just over 1.0 is covered in the experiment. It is calculated from the plenum pressure (p_0) and the ambient pressure (p_a) via the equation, $M_j = (((p_0 / p_a)^{(\gamma-1)/\gamma} - 1)\frac{2}{\gamma-1})^{1/2}$, where γ is the ratio of specific heats for air.

3. Results

3.1 Noise characteristics:

Figure 3 shows comparison of SPL spectra between the flush exit case ('Flsh'), and the no-insert baseline case ('Bsln'), at four values of M_j. The overall sound pressure level (OASPL) in dB is shown on the last column of the legend. The plastic inserts withstood the high pressure flows and the spectra for the subsonic cases were free of significant tones. The spectral peak seen in Fig. 3(d) at M_j =1.09 is due to screech tone. The Flsh insert reduced the screech amplitudes. Importantly, a large reduction of the spectral amplitudes on the low frequency end is noted at all M_j. It can be estimated that the reduction in amplitude due to the area change (11% reduction in equivalent diameter) should be about 1.3 dB. The amplitudes on the low frequency end have reduced in excess of 5 dB and thus cannot be due only to area change. The noise reduction with various septa inserts is shown next.

Spectral data with all other inserts were obtained at the same four values of M_j as in Fig. 3. For brevity only data at M_j =1.00 are shown in Fig. 4. Here, the spectra for all other cases are compared individually with the Flsh case. The spectra with Tab3 case (see Fig. 2) were found to be similar to that for Tab2 case and thus are not shown. A comparison with Bsln data (Fig. 3) shows that all inserts reduce noise, however, the largest reduction is achieved by the Flsh case. The scalloped and the tab cases produced almost the same result as the Flsh case. Similar observations were made at other values of M_j.

While the data in Figs. 3 and 4 pertain to the broad side of the nozzle (microphone on minor axis, ϕ=0°), an example of data for the narrow side (microphone on major axis, ϕ=90°) is shown in Fig. 5(a). Data for the Flsh and Bsln cases are compared at M_j =1.00, for the polar location θ=90°. With reference to Fig. 3(c), it can be seen that very similar noise reduction has occurred also at this ϕ location. Similarly, the comparison at a shallow angle, θ=25° (ϕ=0°), is made in Fig. 5(b). A large noise reduction on the low-frequency end is also noted at the latter polar location.

A brief experiment was conducted in the AAPL. The same NA8Z nozzle with the Flsh insert was used. Spectral data, from 24 polar locations (microphones on the minor axis plane, ϕ=0°), is shown in Fig. 6 for M_j =0.99. The data (power spectral density referenced to 1 ft distance) are shown as a 'carpet plot'. Note that the amplitude difference between the Bsln and the Flsh cases ('dPSD' in dB) is also superimposed in this plot with color code, as indicated in the legend. Large decrease in the amplitudes (green-blue region) is noted on the low frequency end. The trend persists at all polar (θ) locations. Direct comparison of the spectral data between the Bsln and the Flsh cases are shown in Fig.7. The data on minor axis plane shown in Fig. 7(a) may be compared with the data in Fig. 3(c). Similar trends are observed. Data on the major axis plane are shown in Fig. 7(b) and the trends compare well with the data in Fig. 5(a). Thus, the noise suppression by the septa (Flsh) case first observed qualitatively in CW17 is confirmed by the accurate AAPL data.

In the AAPL test, data were also taken at a few other 'set points' (different M_j). Another plot is shown in Fig. 8 for M_j =0.51, with data from an azimuthal array of microphones – all located on the θ=90° plane. Spectra for different

ϕ are shown as a carpet plot and here the legend simply denotes the amplitude of the PSD. It is readily seen that a tone occurs in certain ranges of ϕ. This tone was missed in the CW17 experiment since most data prior to the AAPL experiment were taken on the minor axis plane (ϕ=0°). A dotted line is drawn around the latter ϕ in Fig. 8 for reference. It can be seen that the tone is absent at that location but it is prominent on the major axis plane (ϕ=90°) and certain other ϕ locations, at this low value of M_j.

When the orientation of the nozzle was changed in CW17 (to the configuration shown in Fig. 1a), so that the overhead microphones were situated on the major axis plane (ϕ=90°), the tone clearly appeared in the spectra at lower values of M_j. This is discussed further in §3.3. First, flow field data are presented in the next section.

3.2 Flowfield results:
The flowfield data were obtained with a single hot-wire (Fig. 1b) at a low Mach number of M_j =0.265, using the auxiliary blower system described in §2. Figure 9 compares the centerline variation of the mean velocity and turbulence intensity between the baseline (Bsln) and the 6-septa (Flsh) cases. Since the Flsh case had a partition at the center of the exit, the corresponding data were taken somewhat off-center (y/D=0.1). A faster decay of the centerline mean velocity is noted with the septa. The turbulence intensity profile has shifted upstream. The turbulence for this case is lower relative to the baseline data for the entire region downstream of x/D =3. The lower turbulence in the downstream regions is consistent with the noise reduction observed at low frequencies. However, there are variations of the velocities in the lateral (y) direction and the data shown in Fig. 9 provide only a partial picture of the flowfield.

Contours of mean velocity on cross-sectional (y-z) planes are shown in Fig. 10 for four axial locations of x/D = 0.04, 1, 2 and 4. Data for the Flsh case (right column) are compared side-by-side with the Bsln case (left column). Note that only half of the flowfield is measured, y=0 being a plane of symmetry. For these surveys the probe, aligned with the z-axis (vertical), was inserted from the right (so that the wakes from the partitioning walls could be resolved better); Fig. 1(b). The full flow-field was not surveyed with this configuration since a significant part of the probe support would extend into the flow to reach the far side (negative y) of the jet. It is interesting to note a coalescence of the cellular flowfield structure for the septa (Flsh) case. High-velocity flows from the outermost septum and the one next to it gradually migrate towards each other to form a single cell by x/D =2. The region of high-velocity on the right half of the symmetry plane persists at x/D =4. There is a continual migration of all of the high-velocity flow towards the centerline of the jet. An asymmetry in the flowfield can be noted; the structure of the high-velocity cell near the symmetry plane (y=0) is not clear from these plots.

In order to obtain a clearer understanding, the full flowfield for the Flsh case was then surveyed at x/D=2. This was done by rotating the nozzle 90° (to minimize the probe interference). Mean velocity contours are shown in Fig. 11(a); (the plot is rotated by 90° to be consistent with Fig. 10). It becomes clear that the six high-velocity cells occurring at the nozzle exit have coalesced to form three distinct cells. For some reason the entire flow has migrated to the left and thus the middle cell in Fig. 11(a) is not centered at y=0. This asymmetry is thought to be due to small irregularities in the 3-D printing process. The sensitivity of the flow to the internal flow path is underscored by another set of data taken with the design II 6-septa case, shown in Fig. 11(b). Recall that a septum in design I has rectangular-circular-rectangular passage whereas that in design II has rectangular passage throughout (Fig. 1d). Note also that with 6 septa, the exit geometry was identical with the two designs. With design II, in Fig. 11(b), there is no pairing and the six cells can still be discerned at the measurement location. The lateral spread (in z) is also less. Noise from this case was briefly explored and the reduction (relative to the Bsln case) did not appear as much as seen for design I (Fig. 3). The internal flow-paths thus can have a profound impact on the flow as well as noise. (Design II nozzles yielded some spurious tones at high Mach numbers probably due to structural modes. Both noise and flowfield will be studied further in the future. The only other data with design II nozzles is at the end of the paper with regards to the effect of the number of septa on tones due to vortex shedding from the partitions).

The coalescence of the cells in design I case is likely to be due to an interaction of streamwise vortices in the flow. Secondary flow through a septum, transitioning from circular to rectangular cross-section, may yield pairs of

streamwise vortices. In a limited space, like-signed vortices from alternate pairs would coalesce. The coalescence seen in Fig. 11(a) is reminiscent of the effect of six tabs on a circular nozzle where the flow downstream adjusted as if there were only three tabs [6]. The vorticity distribution and their interaction will also be investigated further in the future.

Spanwise profiles of velocities on the center-plane (z=0), corresponding to the cases of Fig. 10, were obtained in separate runs covering more number of x-stations. These data are shown in Figs. 12 and 13 for the Bsln and the Flsh cases, respectively. In each figure, the mean velocity profiles are shown on the left while the turbulence intensity profiles are shown on the right. For the Flsh case, the cell migration and pairing can be observed. Note that by x/D =8, the peaks in $U(y)$ profile have practically disappeared. Figure 14 compares y- and z-profiles at x/D =16 through the centerline of the jet, for both the Flsh and Bsln cases. Even though the turbulence profiles exhibit some difference, the mean velocity profiles in the two lateral directions have become practically identical. Thus, for both cases the highly asymmetric initial flow evolved to become almost axisymmetric by x/D =16.

3.3 Tone due to vortex shedding from trailing edge of partitions:

As stated at the end of §3.1, tones were encountered for the septa cases in CW17 when the nozzle was rotated so that the microphones were on the major axis plane (ϕ=90°). Sound pressure level spectra are presented in Fig. 15 for different septa inserts (of Fig. 2) in comparison to the Flsh case. Data for the Flsh case (red line) is repeated in each of Figs 15(a)-(f) – the individual cases compared in these figures are identified in the legends. There is a clear tone at about 22 kHz for the Flsh case. Similar tone(s) appear with all other inserts. The tone is particularly accentuated with the partition-inside case (Insd; Fig. 15a). The fact that some of the configurations, e.g., Tab1, did not take out the tone was somewhat surprising. Apparently, the tabs were not large enough to disrupt the vortex shedding from the partitions.

The tone was found to be prominent at lower Mach numbers and diminished as transonic conditions were approached. This is illustrated by the spectra in Fig. 16(a) and (b) for the Flsh and the Insd cases, respectively. SPL spectra for different jet Mach numbers are shown in a 'waterfall' pattern. For the Flsh case in (a) the tone disappears for M_j >0.77; for the Insd case in (b) the tone persists at high subsonic conditions and disappears for M_j >0.98. When conducting the flowfield surveys, the tone was also noted in the hot-wire velocity spectra. This is shown in Fig. 17 for a range of low M_j. An inspection suggests that the tone is due to Karman vortex shedding from the trailing edge of the partitions. The Strouhal number calculated using the trailing edge thickness is about 0.2. This is illustrated in Fig. 18. Note that the thickness at the middle of the partition was used where it was the thinnest (there was some thickening towards the outer walls). The thickness ('t' indicated in Fig. 18) was significantly smaller with the Insd case, accounting for the relatively higher frequencies of the spectral peaks in Fig. 16(b) compared to those in Fig. 16(a).

The TE vortex shedding is captured by schlieren flow visualization pictures. In Fig. 19, views for the Bsln case are shown in the major axis and the minor axis planes, in (a) and (b), respectively. Corresponding data for the Flsh case are shown in Fig. 20. In Fig. 20(a), the wakes from the five partitions can be seen indicating Karman vortex street structures. This is further illustrated by close-up views in Fig. 21 for three different values of M_j. In all cases similar vortex streets are visible. Thus, the tone observed with the noise spectra must be due to trailing edge vortex shedding from the partitions. At the highest M_j (=1.09) shocks can also be seen in Fig. 21; the vortex streets are visible even in the presence of the shocks.

As noted with Fig. 15, the shedding tones persisted across the various configurations. In practice, one way to alleviate the problem will be to keep the trailing edges as thin as possible. This way the shedding tone would be at a high enough frequency so as not to affect perceived noise levels significantly. Nonetheless, there may be a limit to this due to boundary layer thicknesses and remedial designs to avoid them would be highly desirable. With design II inserts (Fig. 1d), limited parametric variations were made in an effort to eliminate/alleviate the shedding tone, without success so far. In one case, the trailing edges were made corrugated but this did not have a significant effect; tones apparently scaling on an average TE thickness persisted. In an effort to understand the mechanism, the

number of septa was varied. Two sets of SPL spectra data are shown in Fig. 22 for M_j = 0.54 and 0.70. In each set, data for inserts with 3, 4, 5 and 8 septa are shown. Spectral peaks, corresponding to the shedding tones, around 27 kHz and 34 kHz are prominent for M_j = 0.54 and 0.70, respectively. Note that the tone is practically absent for the 3-septa case and gets accentuated for the case with highest number of septa. With 3 septa, the partitions are widely apart and with 8 septa they are closely spaced. Thus, it appears that there may be a resonant-like interaction when the vortex streets are close to each other and that may be the condition yielding conspicuous peaks in the noise spectra.

Conclusions:

(1) The nozzle with the septa is found to be quieter than the corresponding baseline rectangular nozzle without septa. This observation was confirmed by accurate noise measurements in the AAPL. The noise reduction is most pronounced at low frequencies. Various designs involving different partition geometry were explored. It turned out that the noise reduction was the most with the basic septa design for which the partitions ended flush with the nozzle exit.

(2) Centerline velocity profiles exhibit an upstream shift of the jet development for the septa case relative to the baseline (no septa) case. Downstream of x/D=3 the turbulence intensity is seen to be reduced in the cases with the septa.

(3) The cellular flow structure seen initially for the septa case goes through a curious evolution with downstream distance where adjacent cells pair. Thus, the six cell structure from the 6-septa case yields 3 cells by x/D =2. Farther downstream the three converge into one and by x/D =16 the flowfield is seen to become axisymmetric. It is noteworthy that the septa inserts with a different internal design did not exhibit this pairing behavior.

(4) At relatively lower jet Mach numbers a high-frequency tone is heard. This is shown to be due to Karmann vortex shedding from the trailing edge of the partitioning wall that separates a septum from the adjacent ones. It is noted that the shedding tone becomes less accentuated with fewer number of septa, that is, when the partitioning walls are spaced farther apart. This suggests that a resonant like interaction may be in play that produces the sharp tones.

Acknowledgement:
Thanks are due to Adam Wroblewski for help with the 3-D printing of the septa inserts. Support from the AATT Project of NASA's Advanced Air Vehicles Program is gratefully acknowledged.

References:

[1] FELDER, J. L., KIM, H. D. AND BROWN, G. V., 2009, "Turboelectric Distributed Propulsion Engine Cycle Analysis for Hybrid-Wing-Body Aircraft", *AIAA Paper* 2009-1132, 47th AIAA Aerospace Sciences Meeting, Orlando, FL, 5 - 8 January.

[2] BERTON, J. J. AND HALLER, W. J., 2014, "A Noise and Emissions Assessment of the N3-X Transport", *AIAA Paper* 2014-0594, AIAA SciTech Conf., , National Harbor, MD, 13-17 January.

[3] ZAMAN, K.B.M.Q., FAGAN, A.F., BRIDGES, J.E. AND BROWN, C.A., 2015, "An experimental investigation of resonant interaction of a rectangular jet with a flat plate", *J. Fluid Mech.*, vol. 779, pp. 751-775. doi:10.1017/jfm.2015.453.

[4] FRATE, F.C. AND BRIDGES, J.E., 2011, "Extensible rectangular nozzle model system", *AIAA Paper* 2011-975, 49th Aerospace Sciences Meeting, Orlando, FL, 4-7 January.

[5] FAGAN, A.F., L'ESPERANCE, D. AND ZAMAN, K.B.M.Q., 2014, "Application of a novel projection focusing schlieren system in NASA test facilities", *AIAA Paper* 2014-2522, 31st AIAA Aerodynamic Measurement Technology and Ground Testing Conference, Atlanta, GA, 16-20 June.

[6] ZAMAN, K.B.M.Q., REEDER, M.F., AND SAMIMY, M., 1994, "Control of an axisymmetric jet using vortex generators", *Physics of Fluids A*, *6*(2), pp. 778-793.

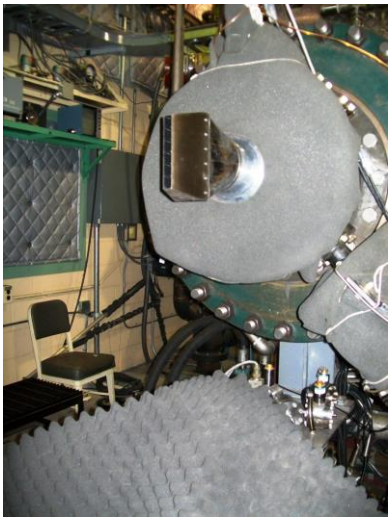

(a)

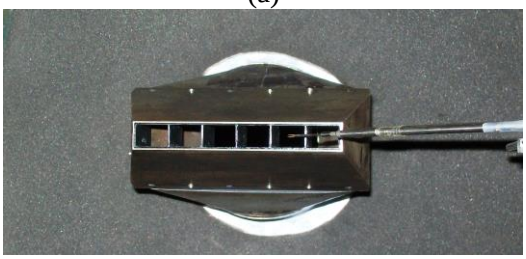

(b)

(c)

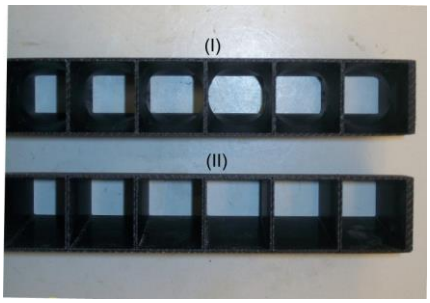

(d)

Fig. 1 Experimental facility. (a) Jet rig with 8:1 aspect ratio nozzle; microphones are located overhead, (b) nozzle with hot-wire setup, (c) picture of various nozzle inserts, (d) views from back of inserts. In (d) top (I) is design where passage through a septum goes through a circular cross-section, and bottom (II) is design where the passage is rectangular throughout.

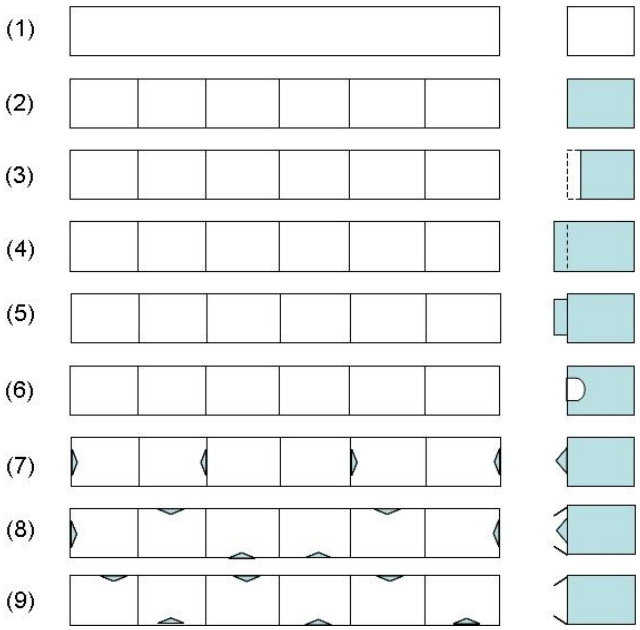

Fig. 2 Schematics of the exit shapes of various inserts with abbreviations for each insert case noted in parentheses: (1) baseline (Bsln), (2) flush exit (Flsh), (3) partition ending inside (Insd), (4) partition protruding outside (OutF), (5) partition protruding outside with trimmed end (OutT), (6) scalloped (Sclp), (7) tab case #1 (Tab1), (8) tab case #2 (Tab2) and (9) tab case #3 (Tab3).

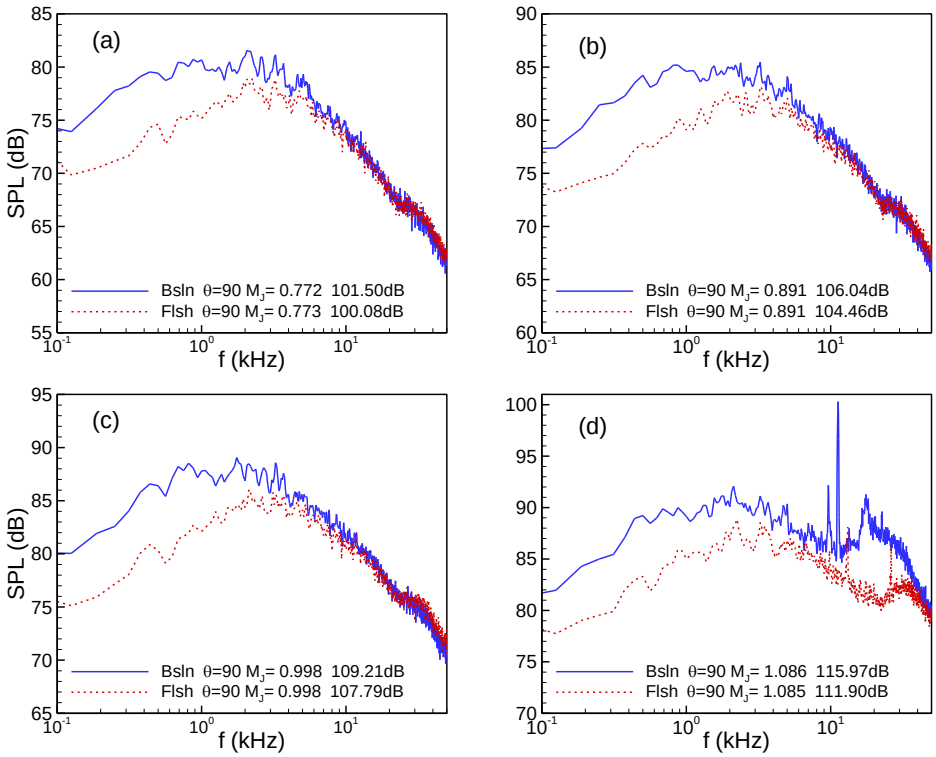

Fig. 3 Comparison of SPL spectra between flush exit case (Flsh: red dashed line) and baseline case (Bsln: blue solid line). Nominal jet Mach number (M_j) is: (a) 0.77, (b) 0.89, (c) 1.00 and (d) 1.09. Microphone located on nozzle's minor axis plane (i.e., on broad side, ϕ=0°), at polar angle θ=90°.

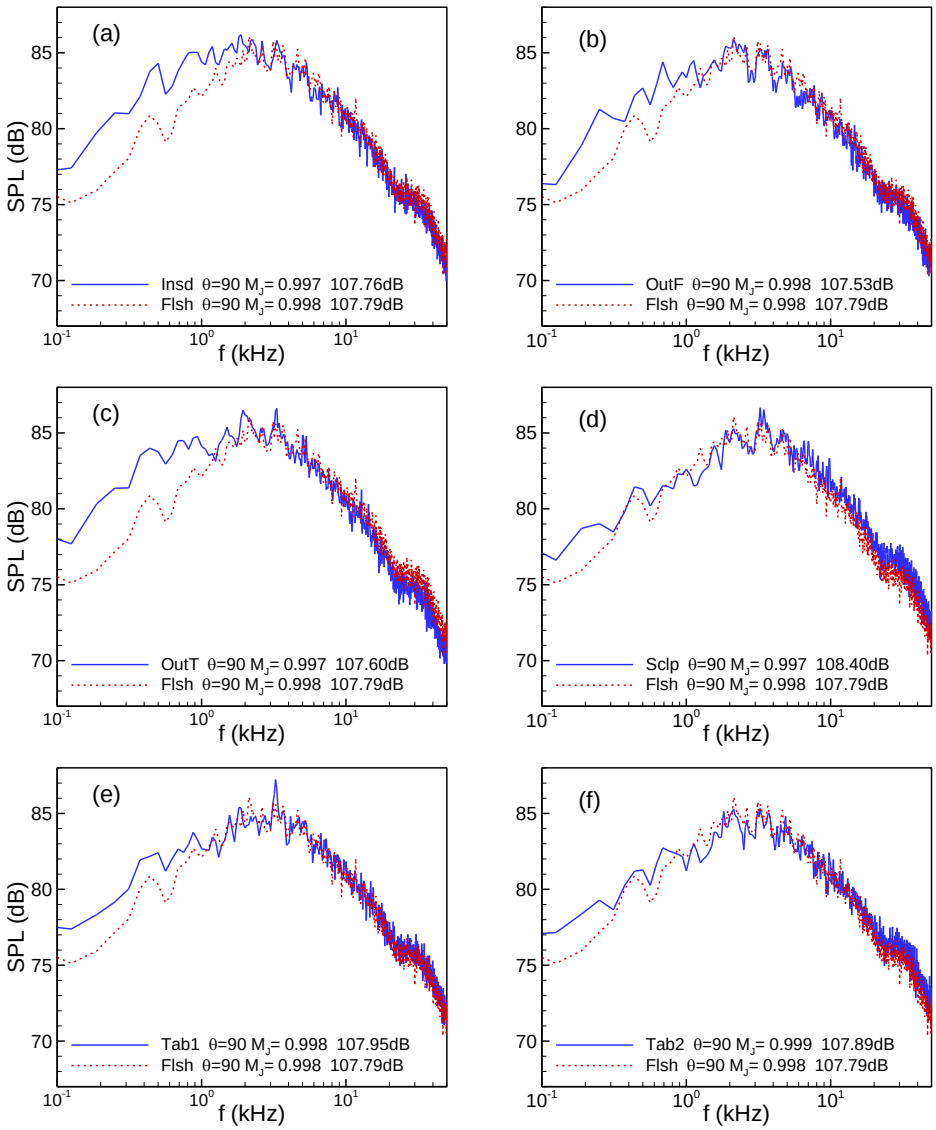

Fig. 4 Comparison of SPL spectra (as in Fig. 3) between Flsh case (red dashed line) and other cases (blue solid line): (a) partition inside (Insd), (b) partition outside (OutF), (c) trimmed partition outside (OutT), (d) scalloped (Sclp), (e) tab1 and (f) tab 2; M_j =1.00.

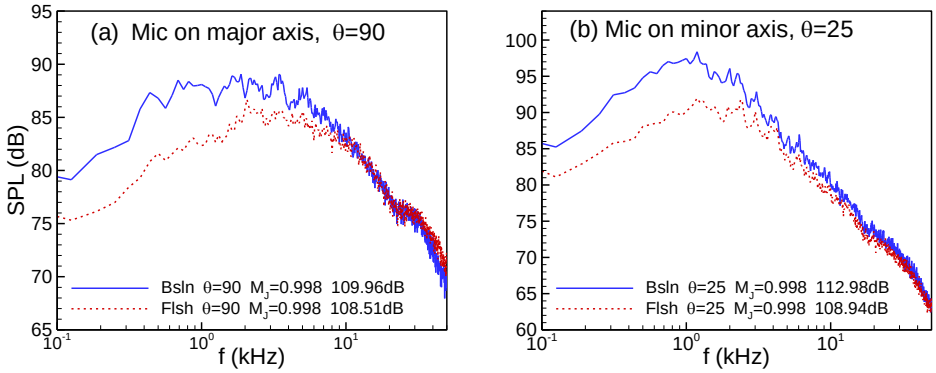

Fig. 5 Comparison of SPL spectra between Flsh and Bsln cases at M_j =1.0; (a) measurement on major axis plane (ϕ=90°), at polar location θ=90°, (b) measurement on minor axis plane (ϕ=0°), at polar location θ=25°.

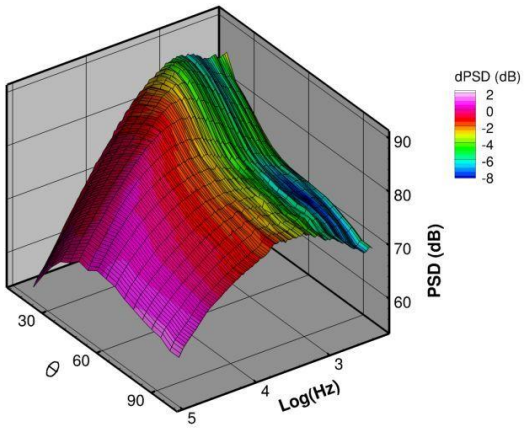

Fig. 6 Power spectral density (PSD) of sound pressure for the Flsh case measured in the GRC AAPL facility. Data for various polar (θ) locations shown as a 'carpet plot'; M_j =0.99. Microphones located on minor axis plane, ϕ=0°; data are 'lossless' and referenced to 1-ft distance. Difference in PSD from baseline case data (dPSD) shown by superimposed color code.

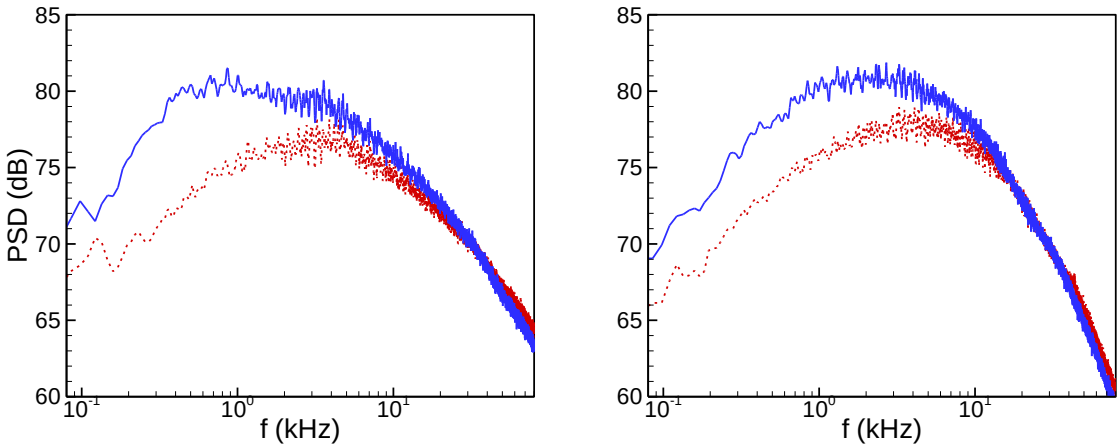

Fig. 7 Comparison of PSD data (Fig. 6) between the Bsln (blue, solid) and the Flsh (red, dashed) cases, at polar location θ=90°; M_j =0.99. (a) Minor axis plane (ϕ=0°), (b) major axis plane (ϕ=90°).

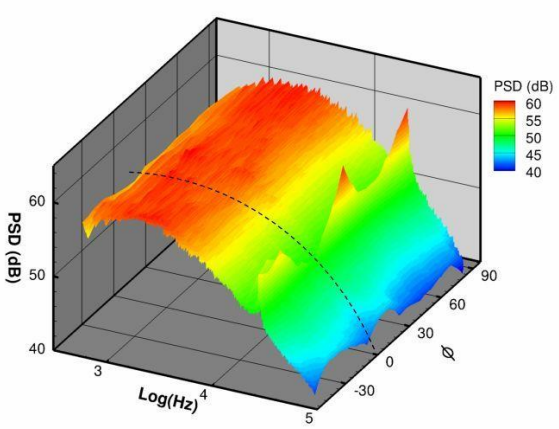

Fig. 8 PSD data as in Fig. 6 for the Flsh case at M_j =0.51. Data shown as a function of azimuthal (ϕ) locations. Location of minor axis plane (ϕ=0°) is marked by a dotted curve. Microphones on θ=90° plane.

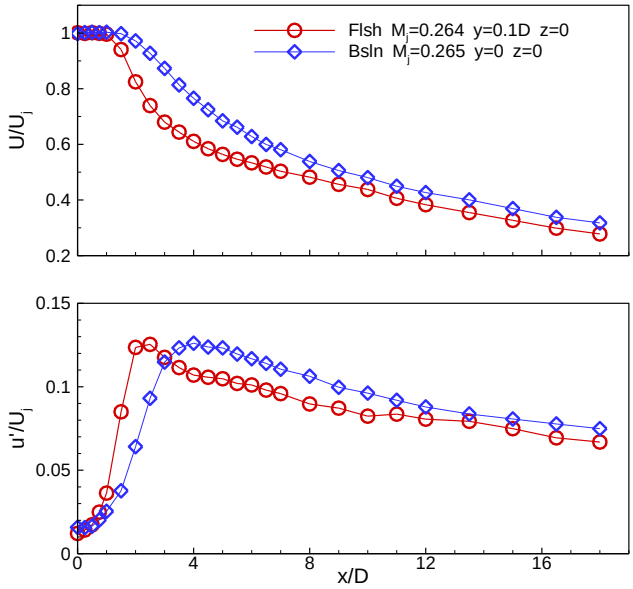

Fig. 9 Comparison of velocity profiles between the Bsln and the Flsh cases taken near the centerline of the jet; M_j =0.265. Top: mean velocity, bottom: turbulence intensity.

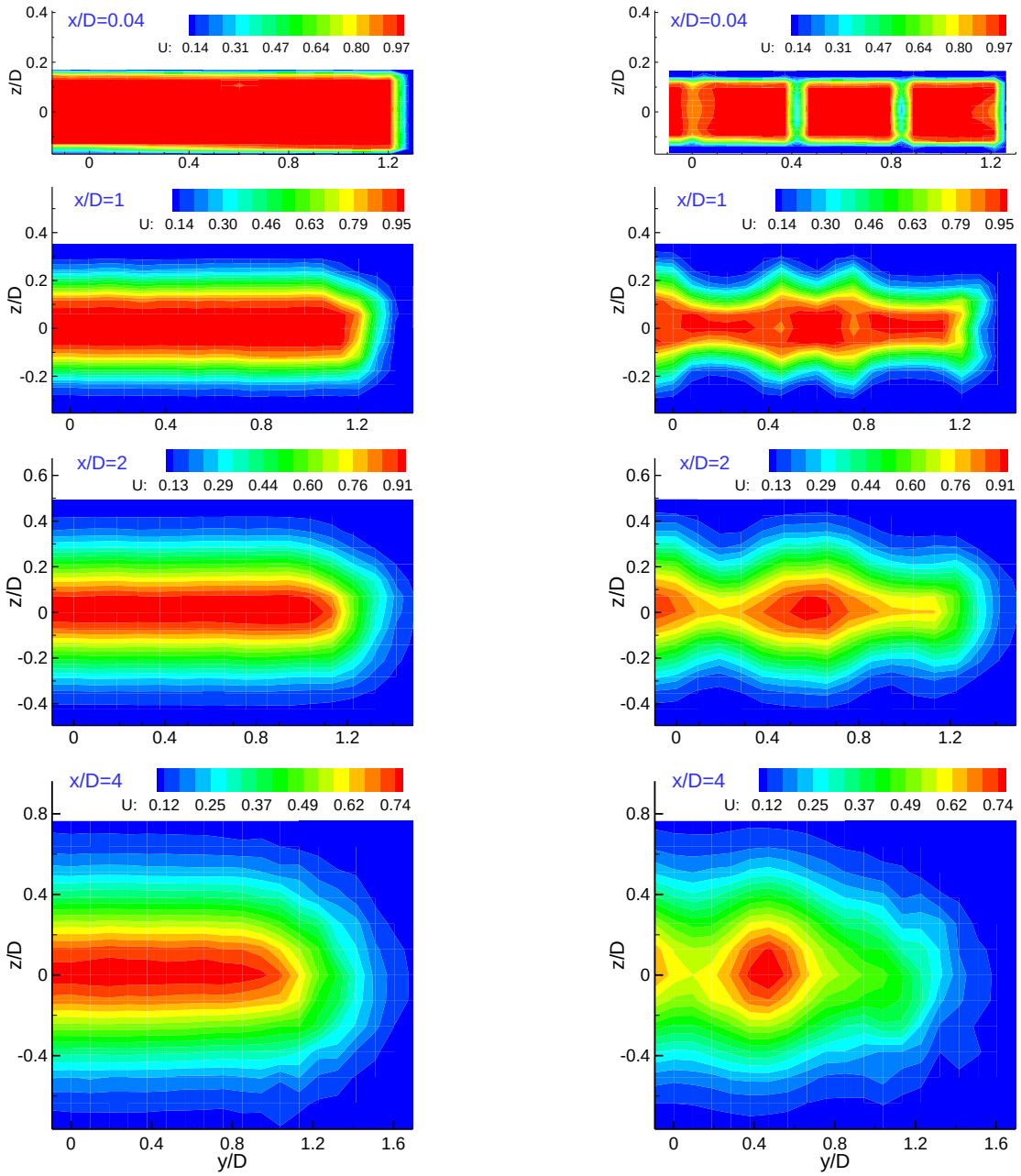

Fig. 10 Mean velocity distribution on cross-sectional plane at different axial locations, as indicated; left column for Bsln case, right column for the Flsh case.; M_j =0.265.

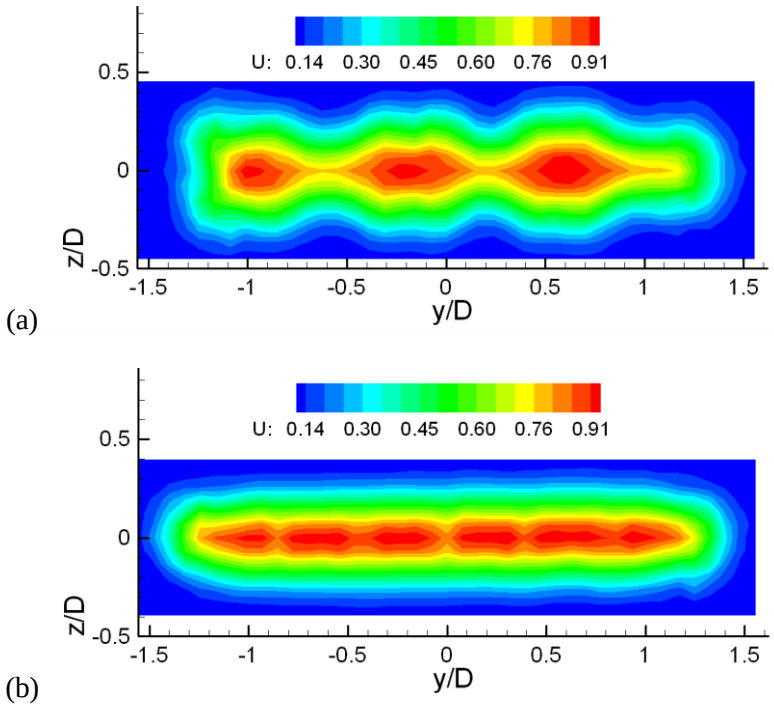

Fig. 11 Mean velocity distribution over full cross-section at *x/D* =2. (a) Data for the 6-septa case (Flsh) with rectangular-circular-rectangular passages (design I, Fig. 1d), (b) data for the new 6-septa case with rectangular passages throughout (design II, Fig. 1d).

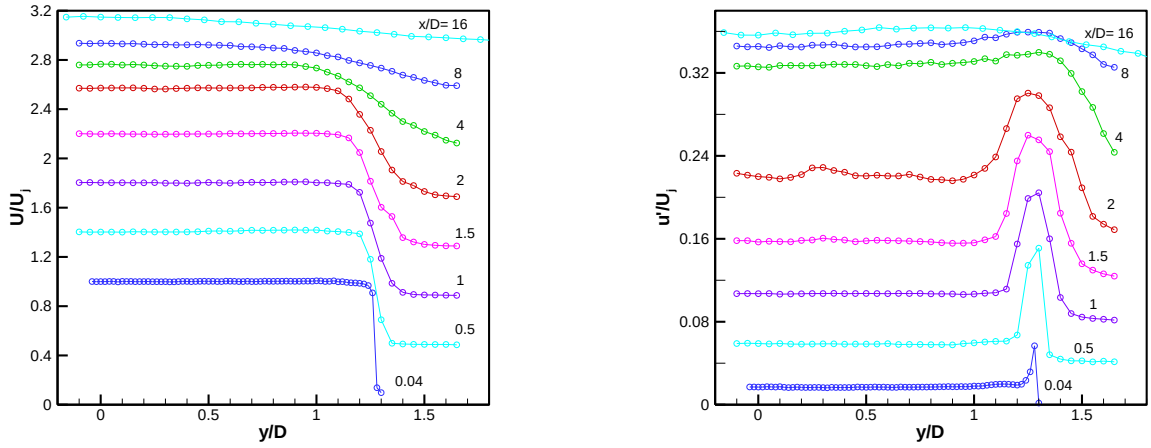

Fig. 12 Streamwise evolution of velocity profiles for the Bsln case; M_j =0.265. (a) Mean velocity, (b) turbulence intensity. In each figure, ordinate pertains to the profile at the bottom and others are staggered by one ordinate division.

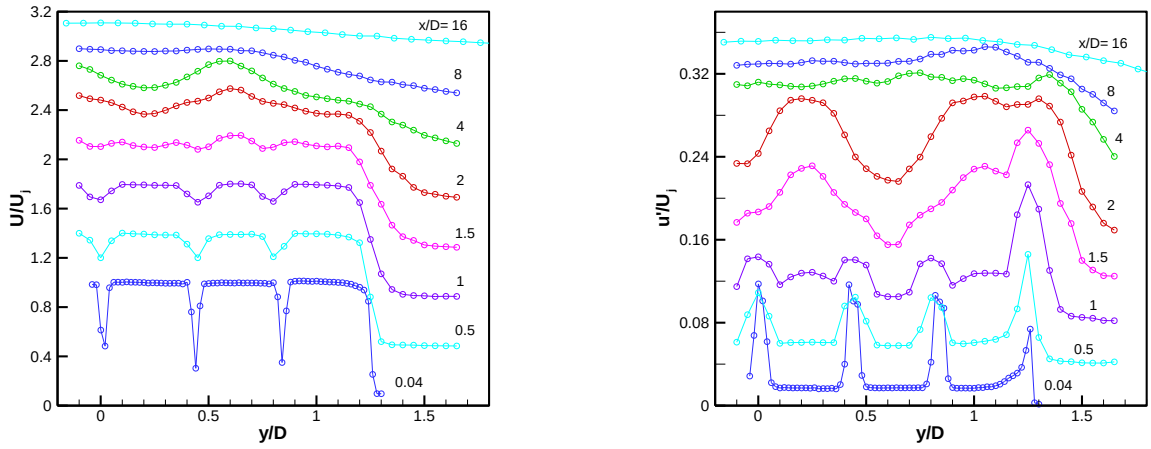

(a) (b)

Fig. 13 Streamwise evolution of velocity profiles for the Flsh case; M_j =0.265. Data shown similarly as in Fig. 12.

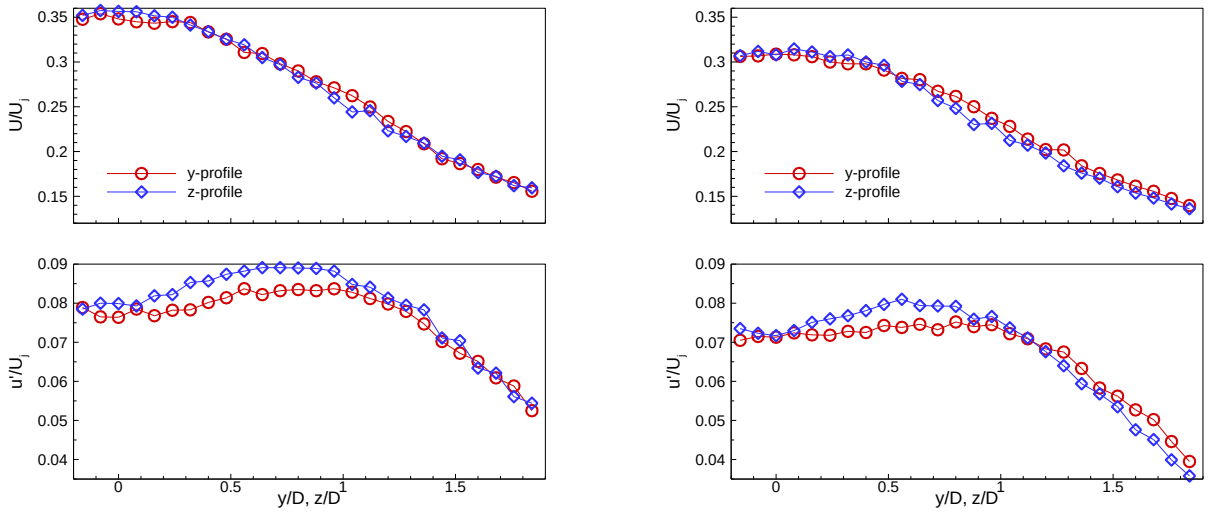

(a) (b)

Fig. 14 Profiles of mean velocity (U) and turbulence intensity (u') at x/D=16; circular (red) symbols for y-profiles (along major axis, z=0), diamond (blue) symbols for z-profiles (along minor axis, y=0); M_j =0.265. (a) Bsln case, (b) Flsh case.

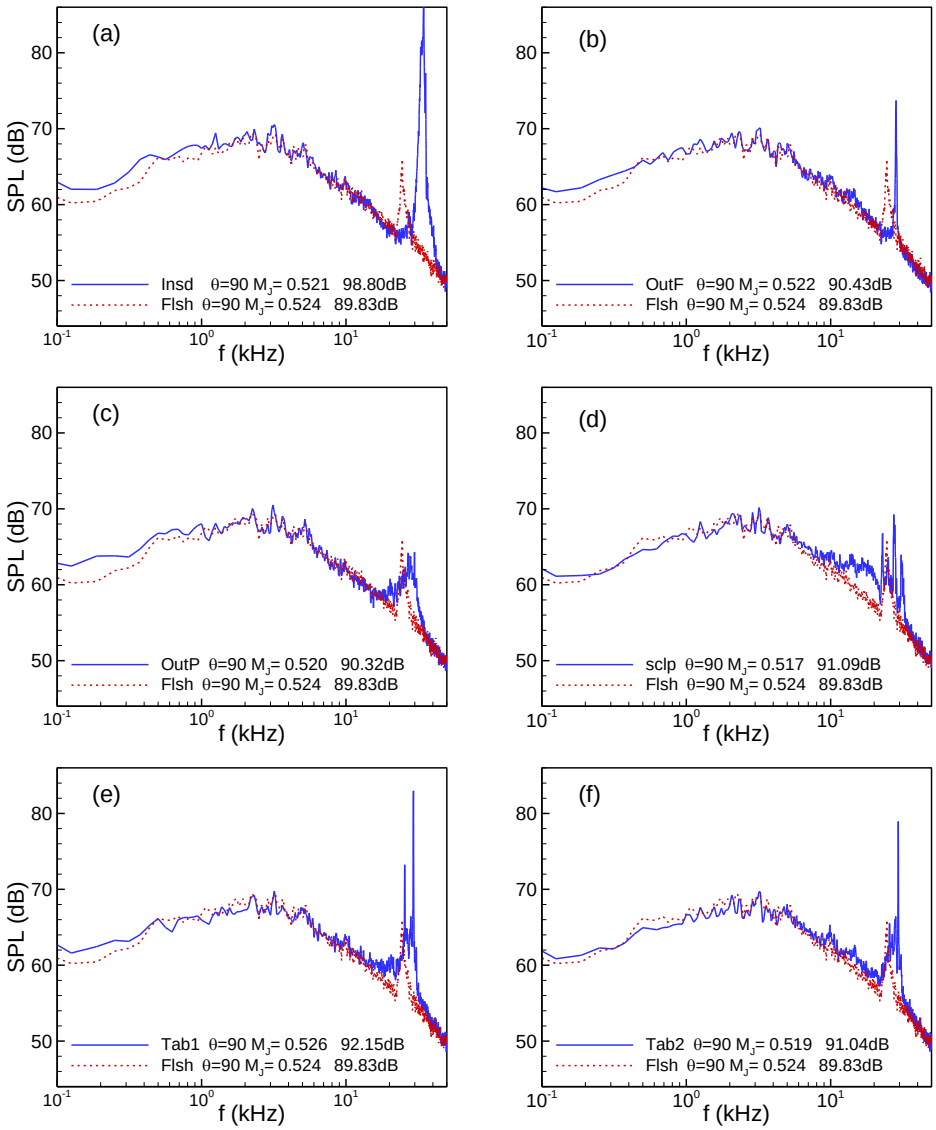

Fig. 15 Comparison of SPL spectra between Flsh case (red dashed line) and other cases (blue solid line), as in Fig. 4; M_j =0.52. Microphone on major axis plane (ϕ=90°). (a) Insd, (b) OutF, (c) OutT, (d) Sclp, (e) Tab1 and (f) Tab2.

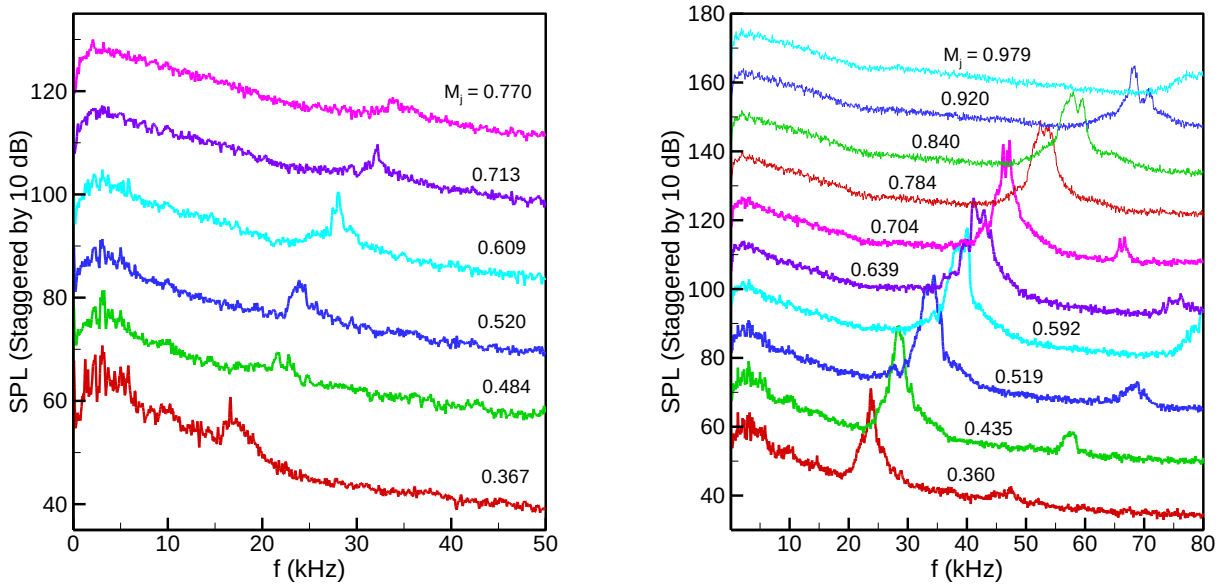

(a) (b)

Fig. 16 SPL spectra at various M_j illustrating partition trailing edge shedding tone; microphone on major axis plane (ϕ=90°). (a) Flsh case, (b) Insd case; (curves are staggered by one ordinate division).

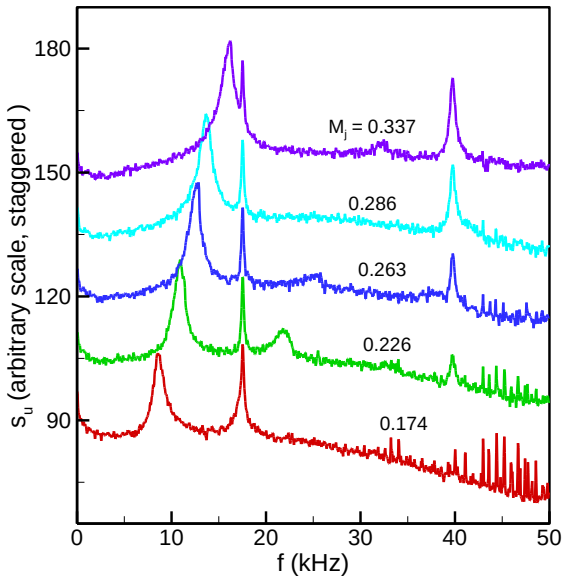

Fig. 17 Hot-wire velocity spectra (s_u) illustrating partition trailing edge vortex shedding for the Flsh case. Measurement just downstream of middle partition; x/D=0.08, y/D=0.03, z=0, ($U/U_j \approx 0.9$). Data shown for five M_j as indicated.

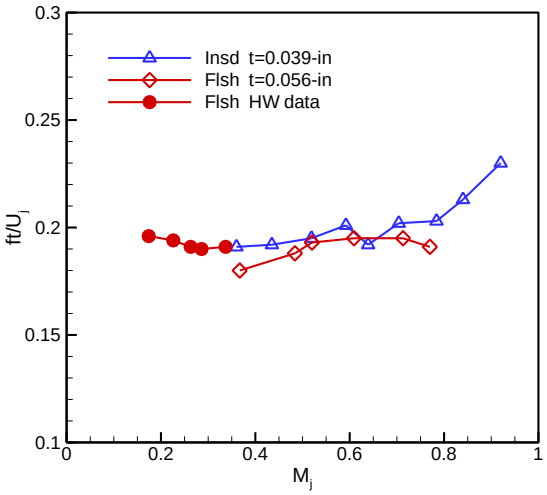

Fig. 18 TE shedding Strouhal number versus M_j based on spectral peaks of Figs. 16 and 17.

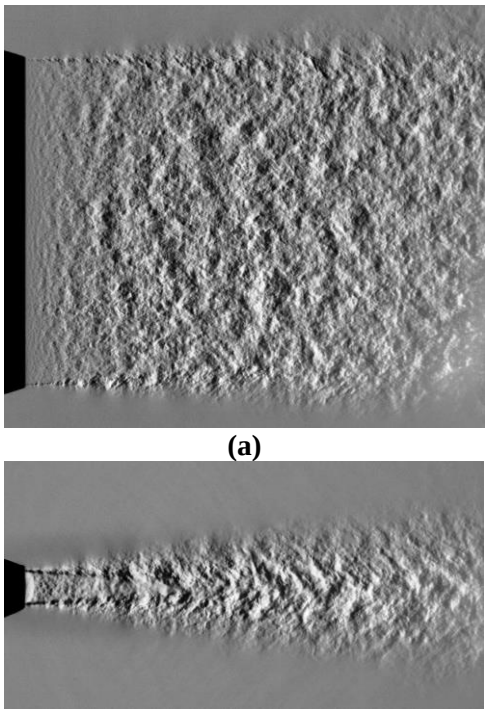

(a)

(b)

Fig. 19 Schlieren pictures of flow for the Bsln case at M_j=1.0: (a) view on major axis plane, (b) minor axis plane.

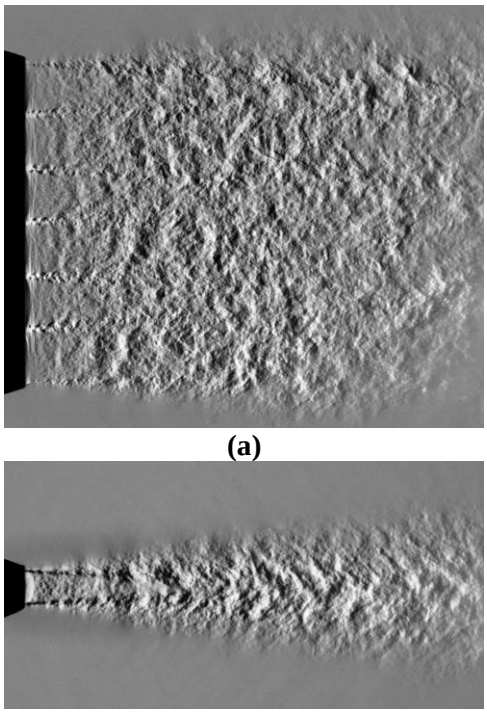

(a)

(b)

Fig. 20 Schlieren pictures of flow for the Flsh case at M_j =1.0: (a) view on major axis plane, (b) minor axis plane.

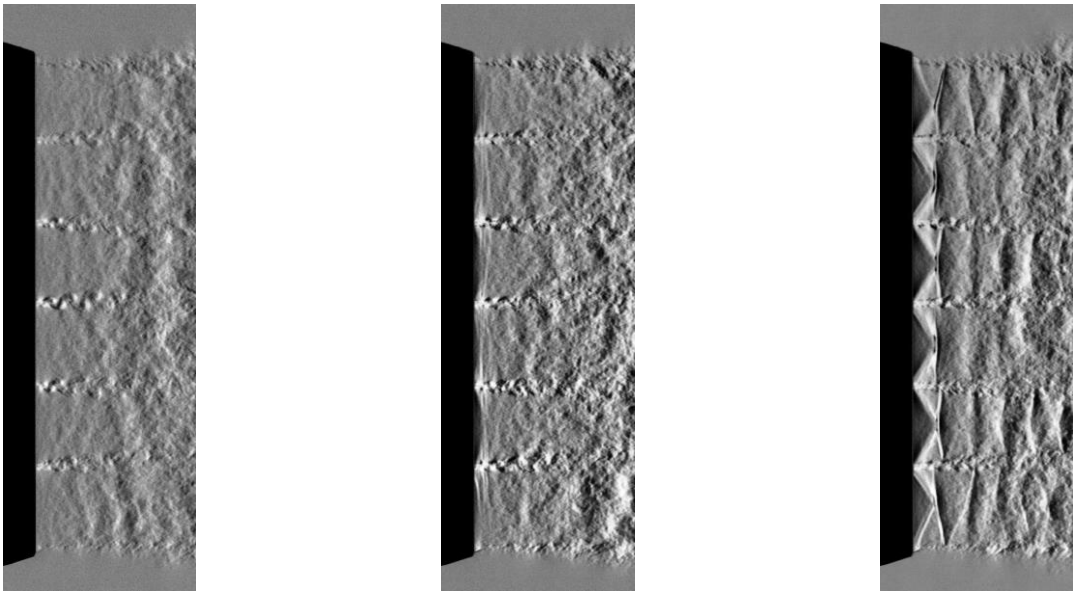

M_j =0.61 M_j =1.00 M_j =1.09

Fig. 21 Schlieren pictures close to nozzle exit for Flsh case at indicated jet Mach numbers.

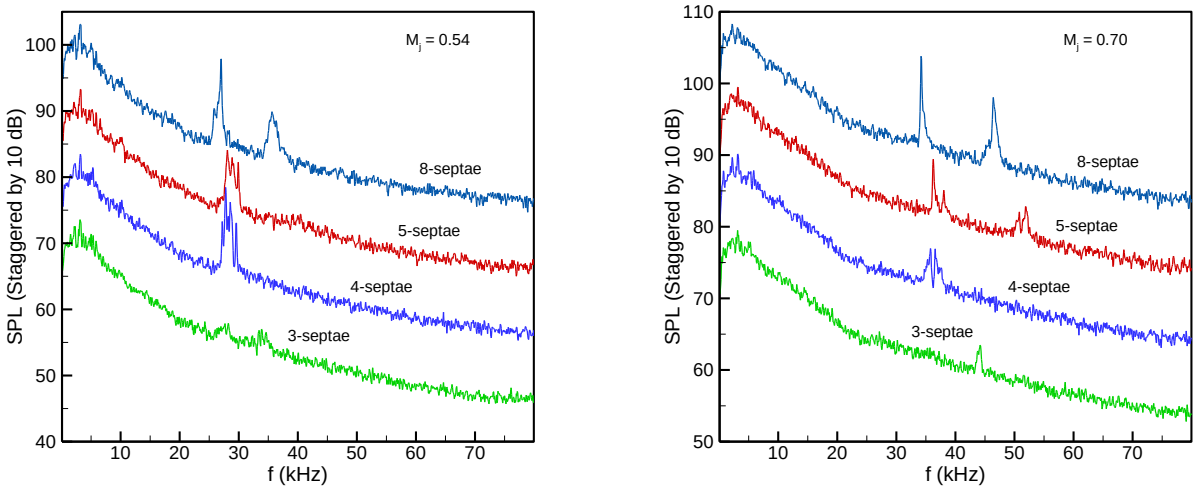

Fig. 22 SPL spectra for inserts with different number of septa, as indicated; ϕ=0°, θ=90°. Data shown for two jet Mach numbers as indicated. Each septum of these inserts have rectangular passage (design II, Fig. 1d).